JOURNAL OF MATERIALS SCIENCE 37 (2002) 5007–5012

Densification behaviour and mechanical properties of pressureless-sintered B_4C–CrB_2 ceramics

S. YAMADA*
Synergy Ceramics Laboratory, Fine Ceramics Research Association, Nagoya, Aichi 463-8687, Japan
E-mail: suzuya-yamada@denka.co.jp

K. HIRAO, Y. YAMAUCHI, S. KANZAKI
Synergy Materials Research Center, National Institute of Advanced Industrial Science and Technology, Nagoya, Aichi 463-8687, Japan

B_4C based ceramics composites with 0–25 mol% CrB_2 were fabricated by pressureless sintering in the temperature range 1850°C to 2030°C. The CrB_2 addition enhanced the densification of B_4C due to the CrB_2–B_4C eutectic liquid phase formation. Both a high strength of 525 MPa and a modest fracture toughness of 3.7 MPa $m^{1/2}$ were obtained for the B_4C–20 mol% CrB_2 composite with a high-relative density of 98.1% after sintering at 2030°C. The improvement in fracture toughness is thought to result from the formation of microcracks and the deflection of propagating cracks resulting from the thermal expansion mismatch of CrB_2 and B_4C.

1. Introduction

Boron carbide (B_4C) based ceramics are useful for various industrial applications because of their outstanding properties such as hardness, elasticity, wear resistance, high melting point and light weight [1–5]. However, poor sinterability caused by low self-diffusivity as well as relatively low strength and fracture toughness places restrictions on their wide application. Fully densified B_4C ceramics without additives are usually fabricated by means of hot-pressing above 2100°C [11], which is relatively expensive and limits sample shape. From such a standpoint, several studies have been conducted to develop a pressureless sintering process for B_4C ceramics.

The addition of carbon has been examined for the purpose of densification of B_4C [6–11]. A specimen with a relative density of 96.4%, which exhibited a flexural strength of 475 MPa and a fracture toughness of 2.8 MPa $m^{1/2}$, was achieved by pressureless sintering and doping with 2 mass% carbon at 2150°C [10]. It was reported that Al, TiB_2 and AlF_3 were effective additives and that a high relative density of 95% was achieved for B_4C ceramics with Al addition pressureless-sintered at 2200°C [12]. The effects of SiC and TiC additives were also investigated, with limited success [11, 13].

Skorokhod *et al*. prepared dense B_4C–TiB_2 composites by reaction sintering B_4C with TiO_2 and C [14, 15]. A flexural strength of 513 MPa and a fracture toughness of 3.71 MPa $m^{1/2}$ were obtained for a B_4C–15 vol% TiB_2 composite sintered at temperatures from 1900°C to 2050°C [14].

Liquid phase sintering is expected to be an alternative method to fabricate dense B_4C ceramics, analogous to the densification of non-oxide ceramics with high covalency, such as silicon carbide and silicon nitride [16, 17]. Relative densities higher than 95% were achieved for a B_4C–TiB_2–1 mass% Fe system by pressureless sintering in the temperature range 2150°C to 2175°C [18]. It was suggested that the liquid phase formed by the iron-rich phase promoted the densification. However, research on the liquid phase sintering of B_4C based ceramics is very limited.

Chromium diboride is expected to be an effective additive for the promotion of liquid phase sintering of B_4C based ceramics, because of the eutectic at 2150°C in the phase diagram of the B_4C–CrB_2 system [22]. In the present study, the densification behaviour of B_4C with CrB_2 was investigated, and the mechanical properties of B_4C–CrB_2 ceramics were evaluated.

2. Experimental procedure

High-purity B_4C powder (Grade 3000F, Elektroschmelzwerk Kempten GmbH, Munich, Germany) and CrB_2 powder (Japan New Metals Co., Osaka, Japan) were used as starting powders. The mean particle size and specific surface area of the B_4C powder were 0.43 μm and 15.3 m^2/g, respectively. The B_4C powder contained oxygen (2.0 mass%), Fe (140 ppm), and Al (50 ppm) as impurities. The mean particle size of the CrB_2 powder was 3.5 μm. The powders were blended using a planetary ball mill with a SiC pot and SiC balls

Now at: Research Center, Denki Kagaku Kogyo K.K., Machida-city, Tokyo 194-8560, Japan.

in methanol. The amount of chromium diboride addition was from 10 to 25 mol%. The slurry was dried in a rotary vacuum evaporator for 1 h, followed by drying at 115°C for 24 h. The powder mixture was passed through a 60-mesh sieve. Green compacts were formed by uniaxial pressing at a pressure of 20 MPa, followed by isostatic pressing at a pressure of 200 MPa. Two types of green compacts were fabricated: (i) discs of dimensions 11 mm $\phi \times 6$ mm for examining densification behaviour and (ii) bars of dimensions 49 mm × 41 mm × 7 mm for measuring mechanical properties.

Pressureless sintering was performed in a graphite crucible using a carbon resistance furnace. Green compacts were sintered at temperatures between 1850°C and 2030°C for 1 h in a flowing Ar atmosphere. The temperature was monitored by an optical pyrometer, which was calibrated in advance using a thermocouple. The heating rates were 40°C/min to 1200°C, 20°C/min to 1500°C and 10°C/min to the sintering temperature. Specimens were cooled down at a rate of 20°C/min. For comparison, monolithic B_4C specimens without any CrB_2 addition were also fabricated using the same procedure.

The densities of specimens were determined by the water displacement method. Theoretical densities were calculated using the rule of mixtures based on the starting composition. In order to observe the microstructure, specimens were polished with diamond slurry down to 1 μm. Microstructural analysis was carried out using scanning electron microscopy (SEM: JSM5600, JEOL Ltd., Tokyo, Japan). For measuring the mechanical properties, test pieces were cut from the sintered specimens and ground with a 400-grit diamond wheel to dimensions of 42 mm × 4 mm × 3 mm. The flexural strength was measured by a four-point bending test with inner and outer spans of 10 and 30 mm, respectively. The fracture toughness, K_{IC}, was measured by the SEPB method [23]. Phase identification was performed by X-ray diffractometry (XRD: RINT 2500, Rigaku Co, Tokyo, Japan) with Cu K_α radiation.

3. Results and discussion

3.1. Densification behaviour of B_4C with CrB_2

Table I summarises starting compositions and their theoretical densities calculated from the densities of each compound. Fig. 1 shows the relative densities of the specimens as a function of the sintering temperature. In the case of the monolithic B_4C specimen, very little increase in relative density could be seen up to a sintering temperature of 1975°C. Above this temperature, the relative density increased slightly with increasing sintering; however, the relative density of the specimen sintered at 2030°C was as low as 60.5%. The relative densities of the B_4C–CrB_2 specimens increased slightly with increasing the sintering temperature up to 1975°C. However, in contrast with the monolithic specimens, significant densification occurred at around 2000°C, and after that, the relative densities increased slightly with increasing sintering temperature. Higher relative densities were obtained for the B_4C with higher CrB_2 contents. A high relative density of about 96% was achieved for the B_4C specimen with 20–25 mol% CrB_2 sintered at 2030°C.

TABLE I Starting compositions and theoretical densities

No.	CrB_2 content			Theoretical density (g/cm^3)
	mol%	mass%	vol%	
1.	0	0	0	2.52
2.	10	12.9	6.2	2.71
3.	15	19.0	9.6	2.82
4.	20	25.0	13.0	2.92
5.	22.5	27.9	14.8	2.98
6.	25	30.8	16.7	3.03

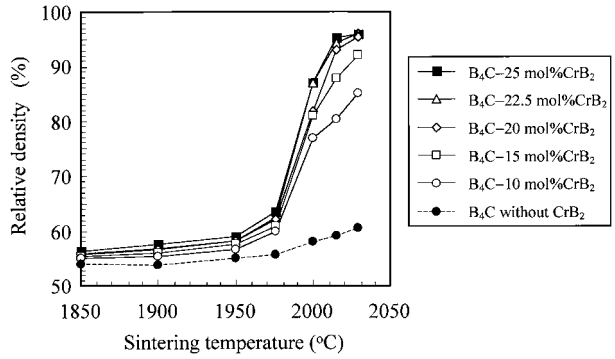

Figure 1 Relative densities of specimens as a function of sintering temperature.

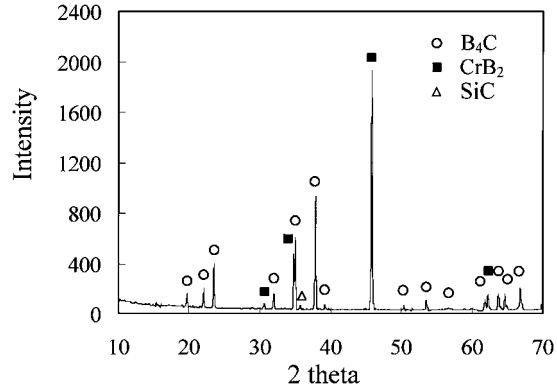

Figure 2 X-ray diffraction pattern of B_4C–20 mol% CrB_2 specimen sintered at 2030°C.

Fig. 2 shows an X-ray diffraction pattern of the B_4C–20 mol% CrB_2 specimen sintered at 2030°C. Only the B_4C and CrB_2 phases were identified, except for a small peak at 35.7°, which corresponds to diffraction from SiC (102). It seems that this SiC contamination originated from the SiC pot and balls during mixing. Therefore, the B_4C–CrB_2 composite specimens were composed of B_4C and CrB_2 phases with a trace of SiC.

Fig. 3, 4 and 5 show the microstructures of the B_4C–CrB_2 specimens sintered at 2000°C, 2015°C and 2030°C. In the photographs, B_4C and CrB_2 phases appear as dark and light areas, respectively, due to the larger atomic weight of Cr compared to B and C. The microstructure of the B_4C–CrB_2 specimens sintered at 2000°C was composed of a B_4C matrix and CrB_2 particles (Fig. 3). The size of the CrB_2 phase of the B_4C–CrB_2 specimens sintered at 2015°C was smaller than that of the specimens sintered at 2000°C and penetrated among fine equiaxed B_4C grains (Figs. 3, 4).

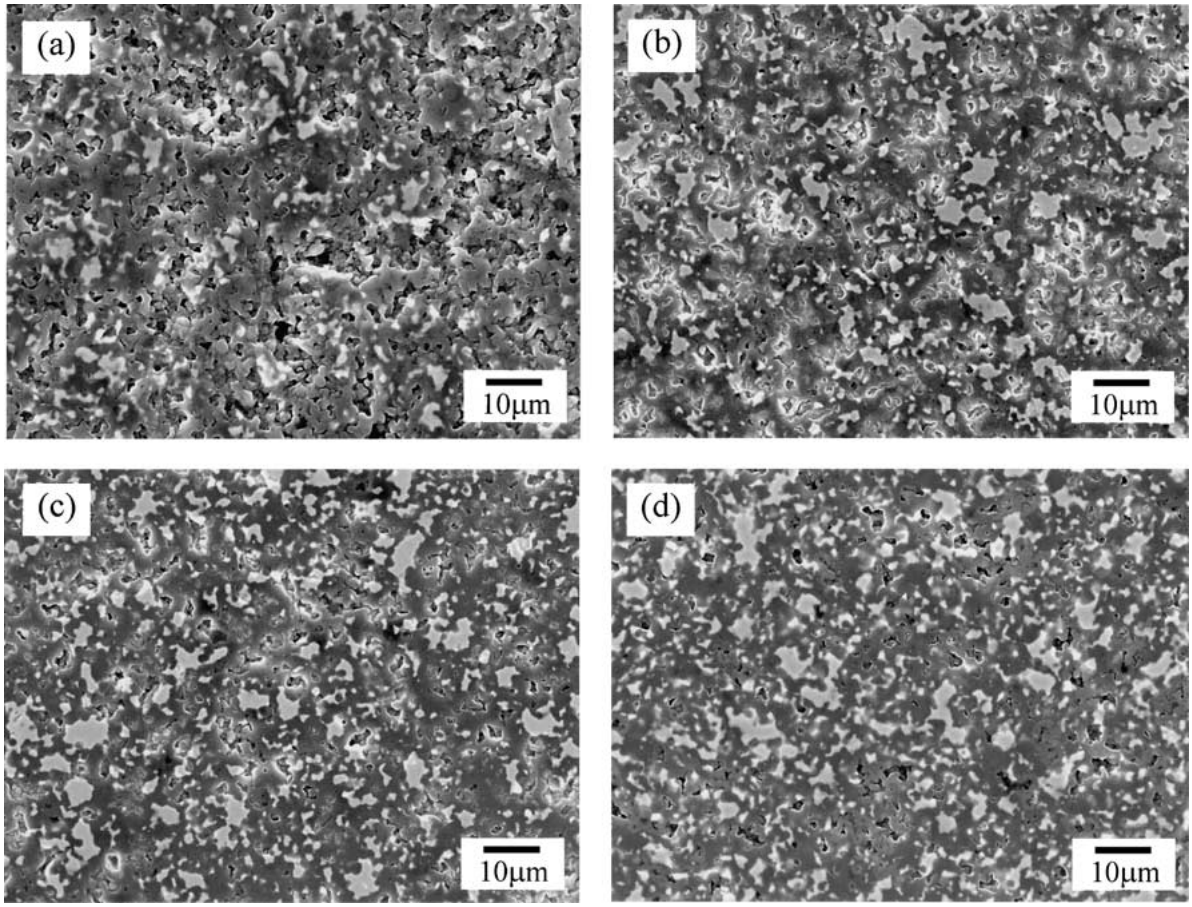

Figure 3 Microstructures of B_4C–CrB_2 specimens sintered at 2000°C: (a) B_4C–15 mol% CrB_2, (b) B_4C–20 mol% CrB_2, (c) B_4C–22.5 mol% CrB_2 and (d) B_4C–25 mol% CrB_2.

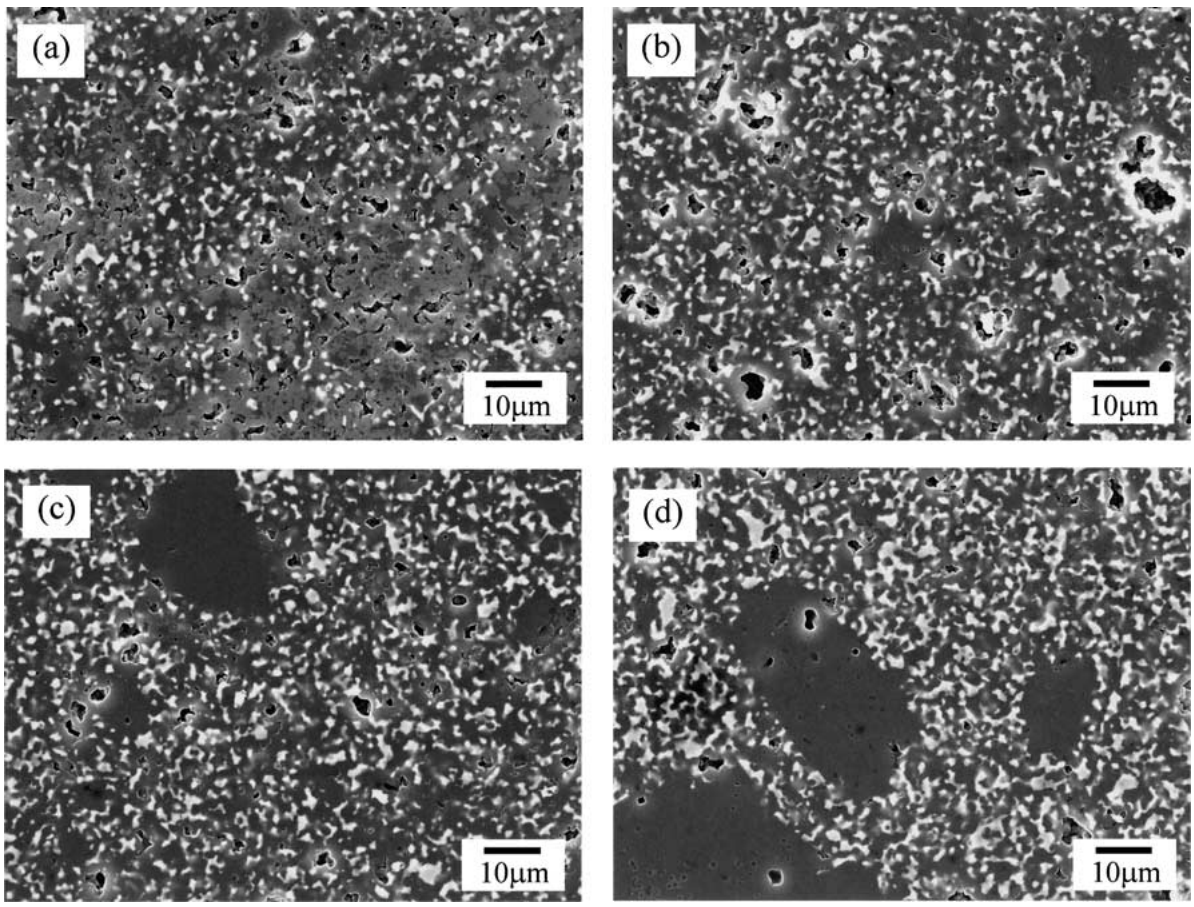

Figure 4 Microstructures of B_4C–CrB_2 specimens sintered at 2015°C: (a) B_4C–15 mol% CrB_2, (b) B_4C–20 mol% CrB_2, (c) B_4C–22.5 mol% CrB_2 and (d) B_4C–25 mol% CrB_2.

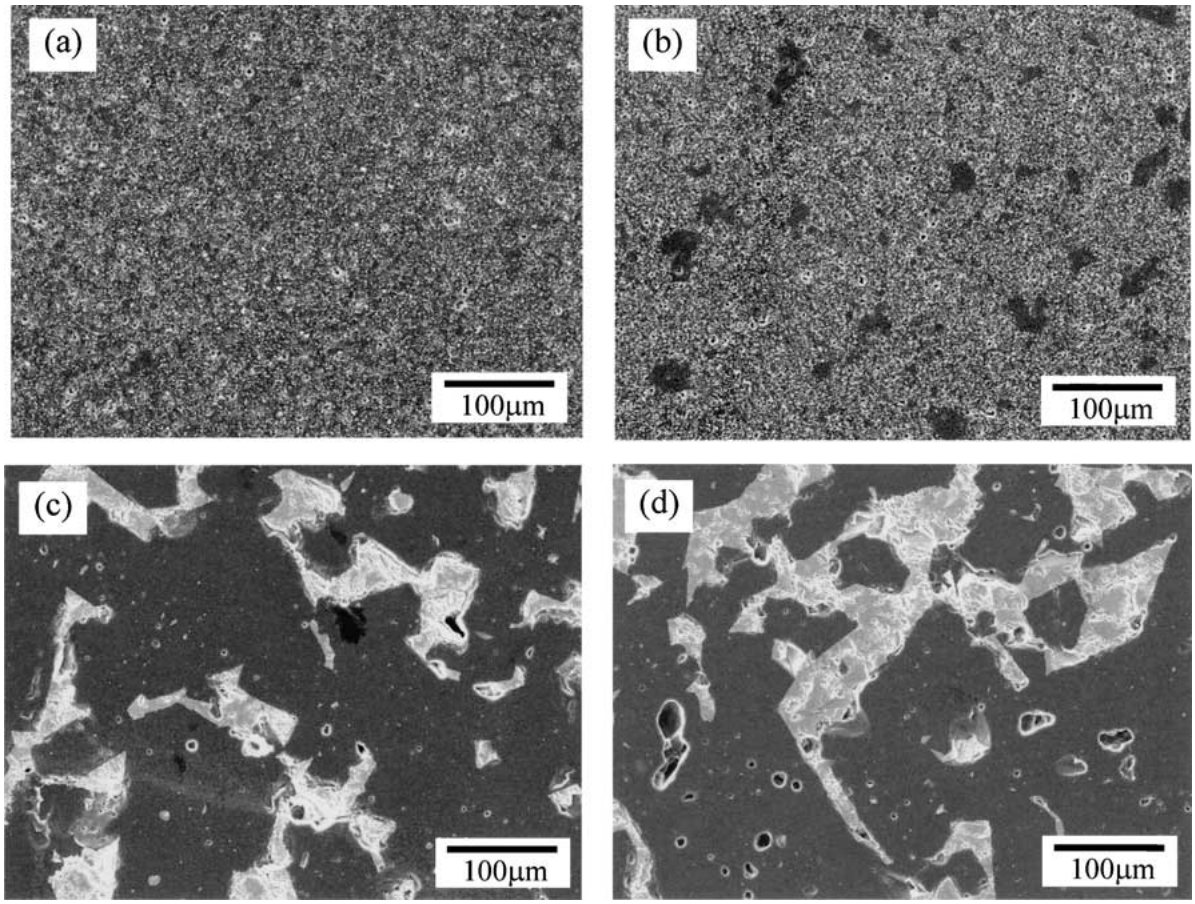

Figure 5 Microstructures of B_4C–CrB_2 specimens sintered at 2030°C: (a) B_4C–15 mol% CrB_2, (b) B_4C–20 mol% CrB_2, (c) B_4C–22.5 mol% CrB_2 and (d) B_4C–25 mol% CrB_2.

Therefore, it is apparent that a large amount of liquid phase formed in the B_4C–CrB_2 system during sintering at 2015°C, although the eutectic temperature for the B_4C–CrB_2 system is 2150°C [22]. It is considered that a lower melting point composition was formed by the reaction with impurities or by a shift in the stoichiometry of B_4C. Some grain growth of B_4C occurred for the specimens with CrB_2 content greater than 20 mol%, with lengths of up to 20–50 μm (Fig. 4c and d). The B_4C composite specimens sintered at 2030°C with 10–15 mol% CrB_2 were composed of fine equiaxed B_4C and CrB_2 phases (Fig. 5a). Some large B_4C grains with a length of about 20 μm could be seen in the B_4C–20 mol% CrB_2 specimen (Fig. 5b). Rapid grain growth occurred for CrB_2 contents between 20 mol% and 22.5 mol%. Huge elongated B_4C grains with lengths up to 100–150 μm could be seen in the B_4C–22.5 mol% CrB_2 and the B_4C–25 mol% CrB_2 specimens, and faceting was evident in the B_4C grains (Fig. 5c and d). Since the abnormal grain growth proceeded at a considerably fast rate, a number of pores remained inside the elongated B_4C grains, hindering full densification.

The marked densification observed at around 2000°C was ascribed to the liquid phase formation. It seems that B_4C particle rearrangement and the B_4C grain growth caused by a large amount of liquid phase gave rise to the increase in densities at sintering temperatures above 2000°C. The increase of CrB_2 content and sintering temperature tended to enhance the B_4C grain growth.

3.2. Mechanical properties of pressureless-sintered specimens

The mechanical properties of the B_4C specimens with 20 mol% and 22.5 mol% CrB_2 pressureless-sintered at 2015°C and 2030°C were measured. Table II shows the densities and mechanical properties of the sintered B_4C–CrB_2 specimens. The relative densities of the B_4C–20 mol% CrB_2 and the B_4C–22.5 mol% CrB_2 specimens sintered at 2015°C were as low as 90.2%

TABLE II Densities and mechanical properties of pressureless-sintered B_4C–CrB_2 specimens

No.	Specimen	Sintering temperature (°C)	Measured density (g/cm^3)	Relative density (%)	Flexural strength (MPa)	Fracture toughness (MPa $M^{1/2}$)
1.	B_4C–20 mol% CrB_2	2015	2.63	90.2	404	2.6
2.	B_4C–22.5 mol% CrB_2	2015	2.78	93.3	400	2.7
3.	B_4C–20 mol% CrB_2	2030	2.86	98.1	525	3.7
4.	B_4C–22.5 mol% CrB_2	2030	2.87	96.3	108	5.8

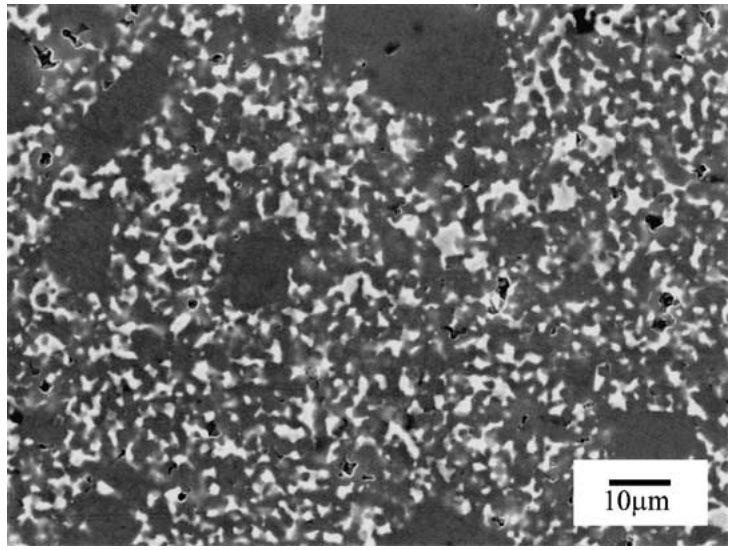

Figure 6 Microstructures of B_4C–20 mol% CrB_2 specimens sintered at 2030°C for measuring mechanical properties.

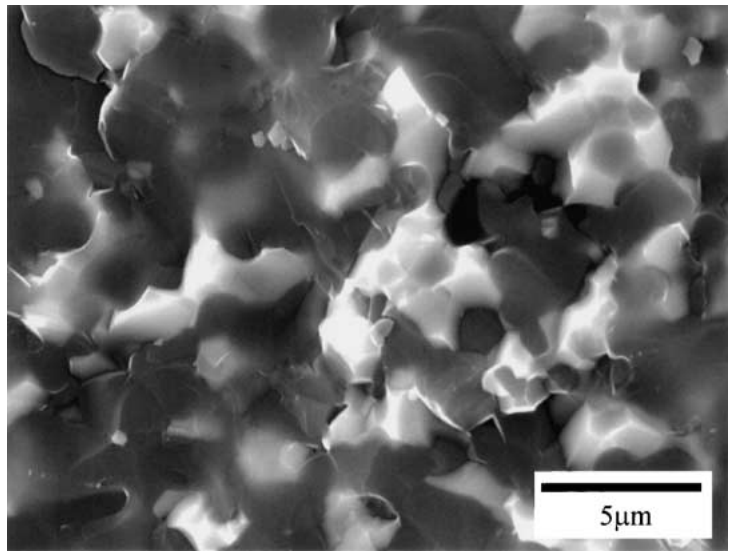

Figure 7 Fractured surface of B_4C–20 mol% CrB_2 specimen sintered at 2030°C.

and 93.3%, respectively. The relatively low flexural strength of approximately 400 MPa and fracture toughness of less than 3 MPa $m^{1/2}$ for these specimens were attributed to their low relative densities. High relative densities of 98.1% and 96.3% were obtained for the B_4C–20 mol% CrB_2 and the B_4C–22.5 mol% CrB_2 specimens sintered at 2030°C, respectively. Both a high strength of 525 MPa and a modest fracture toughness of 3.7 MPa $m^{1/2}$ could be achieved in the B_4C–20 mol% CrB_2 specimen. On the contrary, a low flexural strength of 108 MPa and high fracture toughness of 5.8 MPa $m^{1/2}$ were obtained for the B_4C–22.5 mol% CrB_2 specimen.

Fig. 6 shows the microstructures of the B_4C–20 mol% CrB_2 specimens sintered at 2030°C used for measuring mechanical properties. This microstructure was composed of fine B_4C grains, some grown B_4C grains with a length of about 20 μm, and a CrB_2 phase similar to that shown in Fig. 5b. It seems that the relative high strength of 525 MPa obtained for this specimen was attributed to the high relative density of 98.1% and a microstructure without significant grain growth. The low strength of 108 MPa obtained for the B_4C–22.5 mol% CrB_2 specimen is attributed to the huge elongated B_4C grains with lengths up to 100–150 μm, as shown in Fig. 5c.

The reported fracture toughness of monolithic B_4C is 2.5–2.8 MPa $m^{1/2}$ [10, 25, 26]. In the present work, therefore, the fracture toughness of the composite specimens sintered at 2030°C was improved by the addition of CrB_2. Fig. 7 shows the fracture surface of the B_4C–20 mol% CrB_2 specimen sintered at 2030°C. It can be seen that the B_4C grains fractured transgranularly, whereas intergranular fracture occurred partially at the interfaces between the CrB_2 phase and the B_4C. It appears that the mechanism of improvement in the fracture toughness for these B_4C–CrB_2 specimens is similar to that for two-phase composites with distributed particles such as B_4C–TiB_2 and Al_2O_3-TiC [19–21, 24]. The thermal expansion coefficient of CrB_2 is larger than that of B_4C [1], and, as a result, residual stress is generated around the CrB_2 phase during cooling. It

seems that this residual stress results in the formation of microcracks and, to some degree, the deflection of propagating cracks, leading to improved fracture toughness of the composite materials. It is thought that the fracture toughness for the B_4C–22.5 mol% CrB_2 specimen was further increased to 5.8 MPa $m^{1/2}$ due to the bridging of the huge elongated B_4C grains (Fig. 5c).

4. Conclusions

B_4C–CrB_2 ceramics composites were fabricated by pressureless sintering of powder mixtures of B_4C and CrB_2. The densification behaviour was investigated and mechanical properties were examined. The densification of B_4C was enhanced by the addition of CrB_2 due to the liquid phase formation. A high relative density of 98.1% was achieved for the specimen with 20 mol% CrB_2 sintered at 2030°C. Both a high strength of 525 MPa and a modest fracture toughness of 3.7 MPa $m^{1/2}$ were obtained for this specimen. The thermal expansion coefficient of CrB_2 is larger than that of B_4C, and, as a result, residual stress is generated around the CrB_2 phase. It seems that this residual stress leads to the formation of microcracks and some deflection of propagating cracks, consequently improving the fracture toughness.

Acknowledgments

This work has been supported by METI, Japan, as part of the Synergy Ceramics Project. Part of the work has been supported by NEDO. The authors are members of the Joint Research Consortium of Synergy Ceramics. The authors are grateful to Dr. Shuji Sakaguchi (AIST) for his valuable comments.

References

1. H. NISHIKAWA, *Ceramics* **22** (1987) 40.
2. K. TAKAGI, *Metals & Technologies* **1** (1993) 23.
3. K. NISHIYAMA, *J. Jpn. Soc. Powder & Powder Met.* **43** (1996) 464.
4. W. C. JOHNSON, *Amer. Ceram. Soc. Bull.* **80** (2001) 64.
5. P. LARSSON, N. AXEN and S. HOGMARK, *J. Mater. Sci.* **35** (2000) 3433.
6. F. THEVENOT, *J. Eur. Ceram. Soc.* **6** (1990) 205.
7. *Idem., Key Eng. Mater.* **56/57** (1991) 59.
8. H. SUZUKI, T. HASE and T. MARUYAMA, *Yogyo-Kyokai-Shi* **87** (1979) 430.
9. K. A. SCHWETZ and W. GRELLNER, *J. Less-Common Met.* **82** (1981) 37.
10. K. A. SCHWETZ, L. S. SIGL and L. PFAU, *J. Solid State Chem.* **133** (1997) 68.
11. F. THEVENOT, *J. Nucl. Mater.* **152** (1988) 154.
12. Y. KANNO, K. KAWASE and K. NAKANO, *Yogyo-Kyokai-Shi* **95** (1987) 1137.
13. L. S. SIGL, *J. Eur. Ceram. Soc.* **18** (1998) 1521.
14. V. SKOROKHOD, M. D. VLAJIC and V. D. KRSTIC, *J. Mater. Sci. Lett.* **15** (1996) 1337.
15. *Idem. Materials Science Forum* **282/283** (1998) 219.
16. M. OMORI and H. TAKEI, *J. Amer. Ceram. Soc.* **65** (1982) C-92.
17. E. TANI, S. UMEBAYASHI, K. KISHI, K. KOBAYASHI and M. NISHIJIMA, *Amer. Ceram. Soc. Bull.* **65** (1986) 1311.
18. D. K. KIM and C. H. KIM, *Adv. Ceram. Mater.* **3** (1988) 52.
19. V. SKOROKHOD and V. D. KRSTIC, *J. Mater. Sci. Lett.* **19** (2000) 237.
20. L. S. SIGL and H. J. KLEEBE, *J. Amer. Ceram. Soc.* **78** (1995) 2374.
21. S. TUFFE, J. DUBOIS, G. FANTOZZI and G. BARBIER, *Int. J. Refr. Metals & Hard Mater.* **14** (1996) 305.
22. S. S. ORDANYAN and A. I. DMITRIEV, in "Handbook of Ternary Alloy Phase Diagrams," Vol. 5 (ASM international, OH, 1995) p. 5327.
23. T. NOSE and T. FUJII, *J. Amer. Ceram. Soc.* **71** (1988) 328.
24. M. YASUOKA, M. E. BRITO, K. HIRAO and S. KANZAKI, *J. Ceram. Soc. Jpn.* **101** (1993) 889.
25. S. YAMADA, Y. YOSHIZAWA and M. TORIYAMA, in Proceedings of the 7th International Conference on Ceramics Processing Science, Inuyama, May 2000, edited by S. Hirano, G. L. Messing and N. Claussen (The American Ceramic Society, Westerville, 2001) p. 683.
26. S. YAMADA, K. HIRAO, Y. YAMAUCHI and S. KANZAKI, in Proceedings of the 25th Annual Conference on Composites, Advanced Ceramics, Materials, and Structures: A, Cocoa Beach, January 2001, edited by M. Singh and T. Jessen (The American Ceramic Society, Westerville, 2001) p. 215.

Received 12 April
and accepted 13 August 2002